## DISCLAIMER

**This report was prepared as an account of work sponsored by an agency of the United States Government. Neither the United States Government nor any agency thereof, nor any of their employees, makes any warranty, express or implied, or assumes any legal liability or responsibility for the accuracy, completeness, or usefulness of any information, apparatus, product, or process disclosed, or represents that its use would not infringe privately owned rights. Reference herein to any specific commercial product, process, or service by trade name, trademark, manufacturer, or otherwise does not necessarily constitute or imply its endorsement, recommendation, or favoring by the United States Government or any agency thereof. The views and opinions of authors expressed herein do not necessarily state or reflect those of the United States Government or any agency thereof. Reference herein to any social initiative (including but not limited to Diversity, Equity, and Inclusion (DEI); Community Benefits Plans (CBP); Justice 40; etc.) is made by the Author independent of any current requirement by the United States Government and does not constitute or imply endorsement, recommendation, or support by the United States Government or any agency thereof.**

SAND2025-02310

**SANDIA REPORT**

SAND20XX-XXXX
Printed Click to enter a date

Sandia National Laboratories

# Sensitivity calibration of a Carestream HPX-1 image plate scanner

Greg S. Dunham, Antoinette A. Maestas

Prepared by
Sandia National Laboratories
Albuquerque, New Mexico
87185 and Livermore,
California 94550

Issued by Sandia National Laboratories, operated for the United States Department of Energy by National Technology & Engineering Solutions of Sandia, LLC.



Available to DOE and DOE contractors from
U.S. Department of Energy
Office of Scientific and Technical Information
P.O. Box 62
Oak Ridge, TN 37831

Telephone: (865) 576-8401
Facsimile: (865) 576-5728
E-Mail: reports@osti.gov
Online ordering: http://www.osti.gov/scitech

Available to the public from
U.S. Department of Commerce
National Technical Information Service
5301 Shawnee Rd
Alexandria, VA 22312

Telephone: (800) 553-6847
Facsimile: (703) 605-6900
E-Mail: orders@ntis.gov
Online order: https://classic.ntis.gov/help/order-methods/

## ABSTRACT

There is a need to measure the sensitivity of the image plate scanners used to scan Z shot data. The Carestream HPX-1 image plate scanner was tested, and its performance was characterized to determine the system sensitivity in terms of signal per incident photon as a function of x-ray energy. A Manson source was used to simultaneously expose an Amptek x-ray multi-channel analyzer and image plates, allowing for a comparison of the counts as a function of energy to the signal recorded on the image plates. NIST-certified radioactive sources were used to assign an absolute sensitivity. Results indicate that the HPX-1 scanner response matches the shape of the modeled response, allowing for absolute scaling using NIST-certified radioisotope sources. The HPX-1 scanner shows a stable response with measurements taken over one week. In contrast, the sensitivity of the DITABIS scanner was characterized using the same approach, but it exhibits changes in its response that varied by more than 50% over the span of 4 days.

## CONTENTS



## LIST OF FIGURES

## LIST OF TABLES

This page left blank

## ACRONYMS AND TERMS

| Acronym/Term | Definition |
|---|---|
| $\gamma$ | photon |
| GSU | Gray scale unit |
| IP | Image plate |
| LOS | Line of sight |
| MCA | Multi-channel analyzer |
| MCNP6 | Monte Carlo N-Particle code version 6 |
| NNSS | Nevada National Security Site |
| PMT | Photo-multiplier tube |
| RI | Radio isotope |
| XRD | x-ray detector |

# 1. INTRODUCTION

There is a need to measure the sensitivity of the image plate scanners used to scan Z shot data to provide an absolute calibration. The primary purpose of this work is to characterize the Carestream HPX-1 image plate scanner to qualify the system for use as a replacement when the existing IP scanning systems for Z shot data are no longer functional. In this work, we refer to sensitivity as the relationship between the signal intensity transferred to a digital image file during the scanning process of image plates while preserving x-ray source characteristics. Sensitivity depends on both the intensity and energy content of the x-ray signal that exposes the image plate. In many cases, the signal represents an x-ray spectrum, but it can also consist of image data where size, position, and signal-to-noise ratio are important. To fully understand the data, it must be converted from its raw form of intensity over an x-y grid in pixel space to signal per incident photon resolved over physical space, while also resolving the energy content of the incident spectrum when required. This SAND report will describe the process used in this work to provide an absolute measure of signal per incident photon as a function of energy in an image created by the Carestream HPX-1 image plate scanning system.

The tools used in this work include the new Carestream HPX-1 image plate scanner, a modified Manson source capable of operation up to 30 kV, and an Amptek multi-channel analyzer (MCA) x-ray detector system. The identical process of data collection and analysis was applied to the DITABIS image plate scanner currently used to scan unclassified Z shot data. The details of the experimental setup and the work performed to achieve the measurement precision and repeatability required for this work are described in Section 2. In Section 3, we present the data, analysis approach, and results. In Section 4, we summarize the work and results and suggest future work for consideration. Appendix 1 includes results from previous work to characterize the HPX-1 resolution, contrast, and fade characteristics.

The process used in this work is based on the work by Haugh et al. [1], performed at the Nevada National Security Site (NNSS) Livermore Operations facility in 2013 to characterize image plate scanners for use at the NIF. The same technique was repeated by Rosenberg et al. [2] at the Laboratory for Laser Energetics in 2019 to qualify their image plate scanning systems.

## 2. EXPERIMENTAL SETUP

### Hardware development

A multi-anode Manson source was used to simultaneously expose an Amptek x-ray detector (XRD) and an image plate to study the relationship between the two. The data from the XRD is resolved into counts that are organized into bins as a histogram, to which an energy scale can be applied. The signal from the image plate (IP) is recorded as a signal level per pixel over an x-y grid of pixels. The premise of this work is that if the relative relationship between the two measurements is preserved, the ratio of the measured quantities provides a relative response function, allowing us to measure the quantity of counts per incident photon as a function of photon energy.

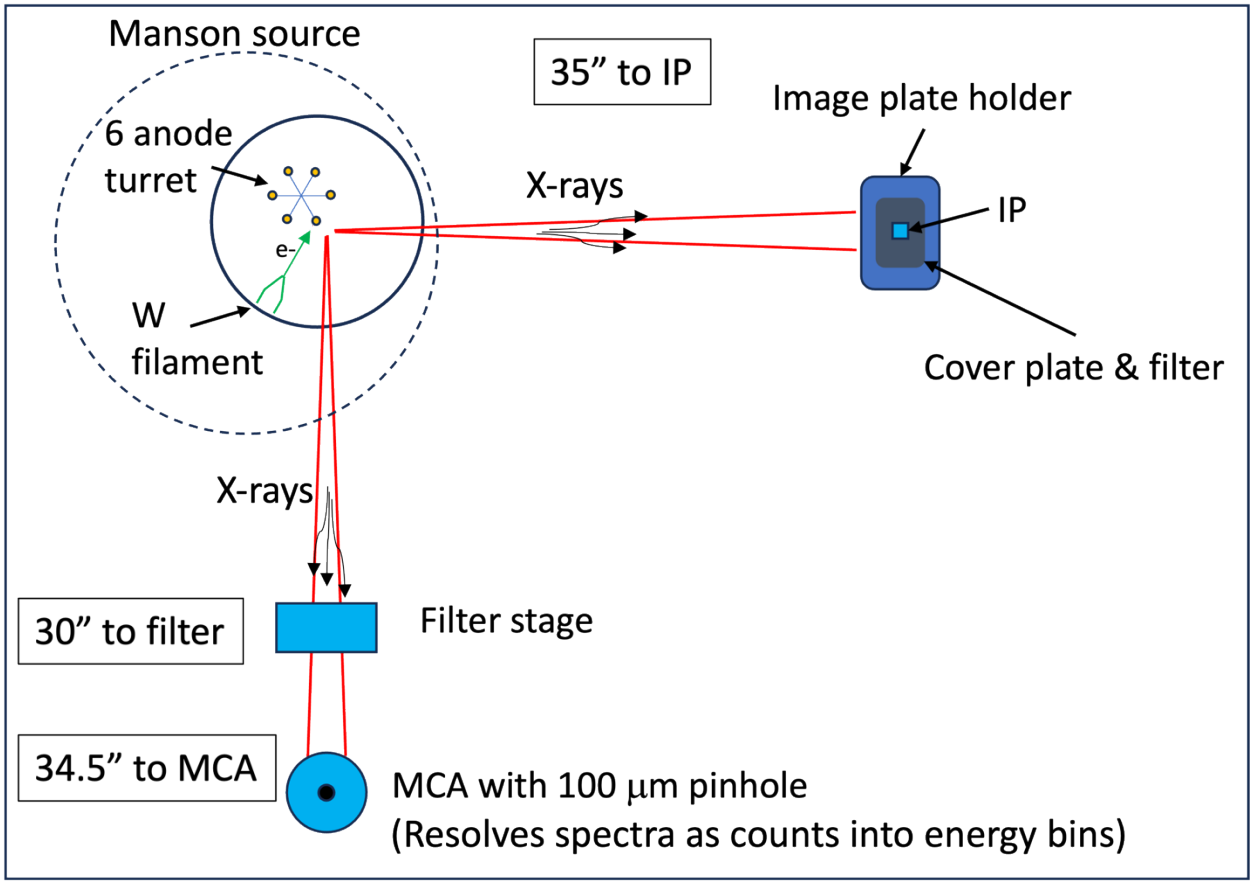


**Figure 1: Experimental setup including the Manson source and two detector arms. One arm exposes image plate to the source while the other exposes the MCA. The entire system is contained within a vacuum environment.**

Figure 1 shows the experimental setup used for this work. The Manson source applies hundreds of microamps of current to a tungsten filament, creating an electron beam focused onto an anode. Anode materials are selected for their respective characteristic K- or L-α emission spectra, which are measured to provide a data point at a specific energy within the desired range. Up to six anodes may be inserted into the turret, allowing quick changes between various energy emission lines without the need to break vacuum. To prevent arcing from electrical breakdown, the system operates under a vacuum of $1x10^{-5}$Torr or better. Two lines of sight (LOS) or arms are available to measure the x-ray emission from the anode material. We assume the emission is uniform into both arms, but the beam shape is likely uniform only over a limited region. Moreover, due to the

unique scattering environment in each arm, the beam at each measurement location is different. The MCA records a collimated signal through a 100 μm pinhole, which limits the number of counts hitting the detector and prevents saturation of the detector electronics. The image plate, in contrast, measures a signal over a larger area, limited only by the size of the image plate and the beam hitting it. However, the beam pattern falls off beyond a limited distance from the beam center. The precise size and shape of the beam pattern intensity depend on the anode material, applied voltage, anode emitting surface state, and the geometry of the system, including LOS distance to the detector and surfaces of the surrounding scattering environment. Through extensive testing, it was determined that we could record a signal over a 1 cm square region around the beam center with relatively uniform signal levels.

To facilitate repeatable placement of the image plate on beam center a test jig was designed to hold the image plate and filter material. The jig is fastened to a breadboard at a repeatable location within the vacuum enclosure. The jig included a front plate which acts as a mask to create the 1 in square region. A slot in the back of the cover plate holds the filter over the exposed region of IP. Figure 2 shows an exploded view of the parts.

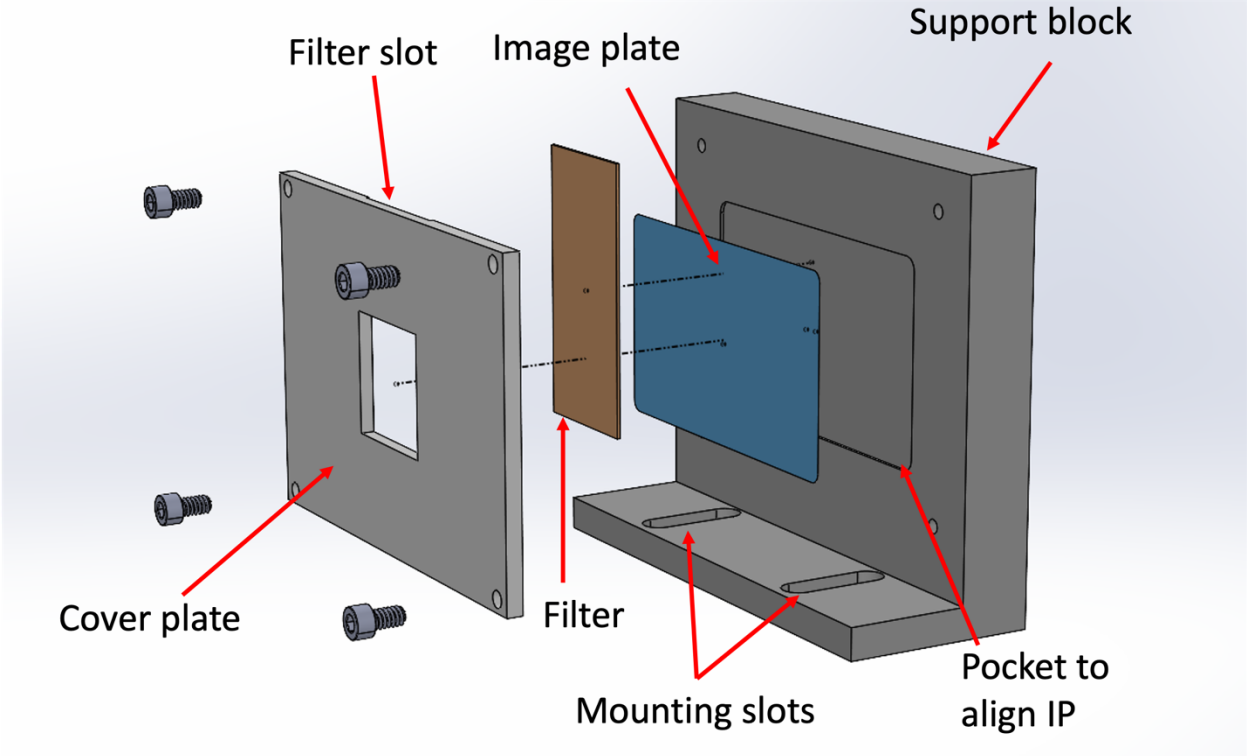


**Figure 2: Exploded view of the test jig used to measure a uniform exposure onto image plates.**

An additional support bracket was designed to hold the MCA on beam center. Figure 3 shows the hardware bolted to a vacuum flange one arm of the Manson source, securing the MCA body to the bracket.

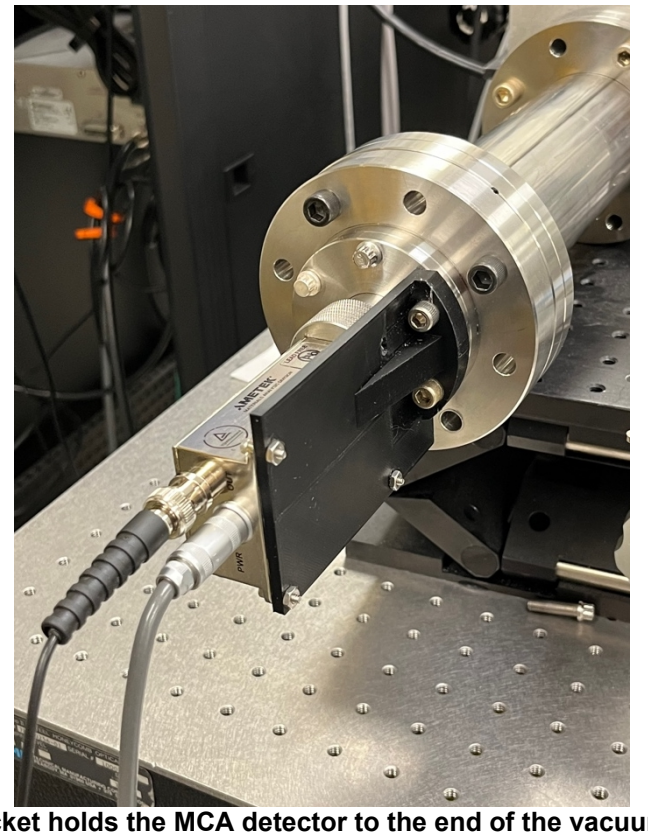


**Figure 3: Support bracket holds the MCA detector to the end of the vacuum flange. This bracket allows repeatable placement on beam center with no movement. Prior to using this bracket count rate would fluctuate by up to an order of magnitude preventing reliable measurements.**

Before using the bracket, the count rate measured at the MCA detector fluctuated by up to an order of magnitude each time the detector was placed into position. Touching or moving the cable connections caused enough movement to skew the pinhole from beam center. In early testing, filtering was applied directly to the front of the MCA snout, overlaying the pinhole. Every time the anode and filter set were changed to measure a different energy point, the location of the MCA and pinhole would change slightly with respect to the beam, rendering repeatability between measurements impossible. This violated the premise of this work, which was that the relationship between the MCA and IP measurements remained unchanged for all datasets collected. A filter stage was added to this LOS, moving the filter closer to the source and removing the need to touch the MCA for all future measurements. Securing the MCA with a bracket precisely located the MCA and pinhole in the same location with respect to the Manson source. These two modifications provided consistency in measurement location for all measurements, allowing us to proceed with data collection.

## Anode selection

Z shot data recorded on image plates ranges in energy from 100's of eV up to many 10's or even 100's of keV. From a practical perspective, however, we limit this determination of response to 100 keV and below. Furthermore, we limit the measurements in this work to less than 30 keV because the Manson source used for this work cannot function above this voltage. The Manson source used

in this work has been modified from its stock form which is limited to operating at less than 8 keV. The anode materials used in this work are Al, Ag, Ti, Fe, Cu, and Zn. Table 1 lists the anode element along with the filter material and thickness, and characteristic line emission and K or L-edge energies.

**Table 1: Anode and filter materials used for this work. Source voltage is the value used for the Manson source. Primary photon energy is the K- or L-shell emission line energy. K or L edge energy denotes the energy of the filter cut.**

| Anode | Filter | Source voltage (keV) | Primary photon energy (eV) | K or L edge energy (eV) |
|---|---|---|---|---|
| Al | 25 μm Al | 3.0 | 1487 | 1559 |
| Ag | 10 μm Ag | 5.7 | 3080 | 3351 |
| Ti | 60 μm Ti | 8.1 | 4620 | 4966 |
| Fe | 100 μm Fe | 14.0 | 6650 | 7112 |
| Cu | 100 μm Ni | 15.8 | 8040 | 8979 |
| Zn | 75 μm Zn | 13.8 | 8637 | 9659 |

These anodes cover the energy range of 1.487 keV to 8.637 keV. We attempted to study additional anodes with higher energy emission lines to provide more confidence in the shape of our response curve. However, results from emissions > 10 keV proved unreliable, showing step increases in response of 2-3 times where a decrease in response was expected. Table 2 lists the additional materials that were used but did not yield acceptable results.

**Table 2: Additional anodes tested which did not provide acceptable results.**

| Anode | Filter | Source voltage | Primary photon energy (eV) | K or L edge energy (eV) |
|---|---|---|---|---|
| Y | 300 μm Y | 24.6 keV | 14958 | 17038 |
| Zr | 250 μm Zr | 26.9 keV | 17668 | 17998 |
| Zr | 300 μm Y | 24.6 keV | 15775 | 17038 |
| Nb | 250 μm Nb | 29.0 keV | 18625 | 18986 |
| Nb | 300 μm Y | 24.6 keV | 16615 | 17038 |
| Mo | 200 μm Mo | 25.0 keV | 17480 | 20000 |
| Ag | 200 μm Ag | 28.0 keV | 22163 | 25514 |

We theorize that the operation and response of the MCA change at higher energies. The detector could be overwhelmed by too high a count rate, leading to increased dead times in the

electronics, which in turn reduces the measured count rate. This condition is typically mitigated by changing pinhole size to further limit count rate; however, doing so would alter the relationship between the MCA and IP measurements. Similar work by Haugh and Rosenberg referenced in [1,2] utilized a photodiode system cross calibrated to an additional absolutely calibrated photodiode, but we did not have this equipment readily available. The referenced work was limited to less than 8 keV.

Furthermore, at higher anode voltages, the beam size and pattern likely change. Considering the long run times of an hour or more, pitting of the anode surface can occur, as shown in Figure 4. This pitting can change the beam pattern over time, potentially contributing to changes in measurement conditions that are difficult to recognize and mitigate, thereby preserving identical conditions for all measurements.

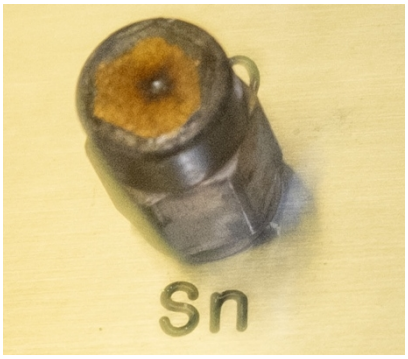


**Figure 4: A tin (Sn) anode showing pitting and discoloration of the anode surface caused from prolonged exposure to high a voltage e- beam.**

## Spectral purity

To achieve spectral purity, the approach taken in this work was to filter a K- or L-shell emission using a suitable filter material with a K-edge just above the desired emission line energy. This method effectively reduces the energy content of the spectrum below the emission line to negligible levels through careful matching of filter thickness. Figure 5 shows an example for Cu K-$\alpha$ emission filtered by 100 $\mu$m of Ni.

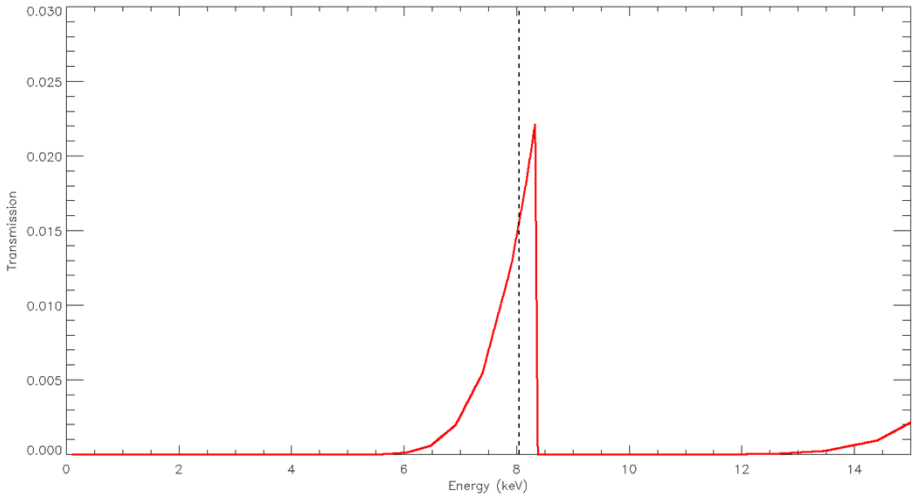


**Figure 5: Model calculation showing where the Ni K-edge would lie in relation to the K-α emission from Cu. Red line: transmission through 100 μm of Ni. Notice the filter transmission is near zero for all but a region around the spectral line of interest marked as the dashed vertical line.**

A balance must be achieved between reducing the undesired spectral content and preserving the desired peak emission. If the filters are too thin, the low-energy content will broaden the energy spectrum of the recorded signal. Conversely, if the filters are too thick, exposure times become excessively long, making it difficult to achieve a useful signal-to-noise ratio on the image plates. For the example case shown in Figure 5 and Figure 6 the required exposure time was 5 minutes, on the shorter end of all samples collected.

Modelling and testing were conducted to achieve the right balance. Anode and filter combinations other than those presented in Table 1and Table 2 were considered, but ultimately, the choice of filter material and thickness was partly determined by product availability. Some choices of more exotic materials were cost prohibitive.

Figure 6 shows both the raw and filtered spectrum recorded for copper with 100 μm of nickel filtering. The 100 μm of Ni filtering allowed for a signal with a weighted mean energy of 8023 eV ± 34 eV for this case.

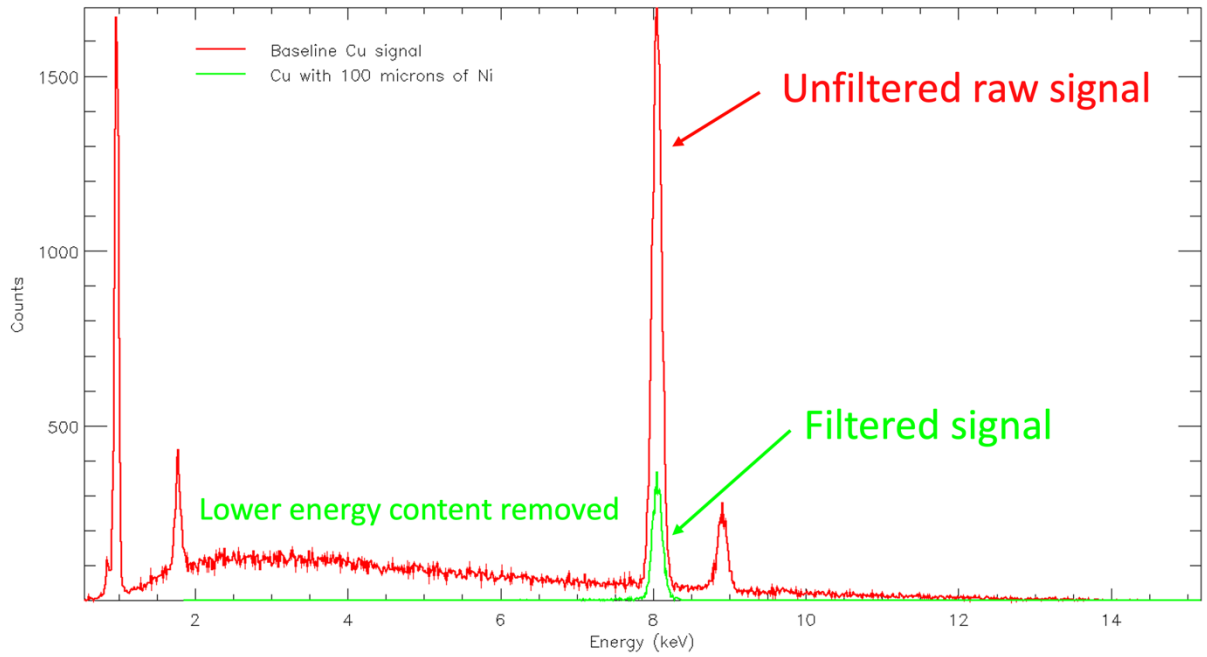


**Figure 6: An example of a spectrally pure measurement from a Cu anode with Ni filtering. The red line represents the raw unfiltered spectrum showing the prominent Cu K-a emission at 8 keV along with other emission lines and substantial Bremsstrahlung. The green curve shows the same emission filtered to remove the undesired energy content leaving only the emission from the K-α emission. The voltage applied to the Manson source was just high enough to excite the desired transition, typically 5-6 keV above the desired emission line.**

## Signal uniformity

Signal uniformity was a concern for the image plate measurements because a relatively large sample area was used compared to the 100 μm diameter pinhole in front of the MCA. If the signal content varied significantly, the corresponding signal level inferred from the data would exhibit high variance. Tests were conducted to determine the optimal positioning of the image plate with respect to the Manson source beam. The design of the test jig placed a 1 cm square region at the beam center, with the jig mounted on a breadboard at a known distance from the source. Figure 7 shows a sample image plate scan along with a histogram of the pixel values, featuring Gaussian fit to measure the width of the distribution.

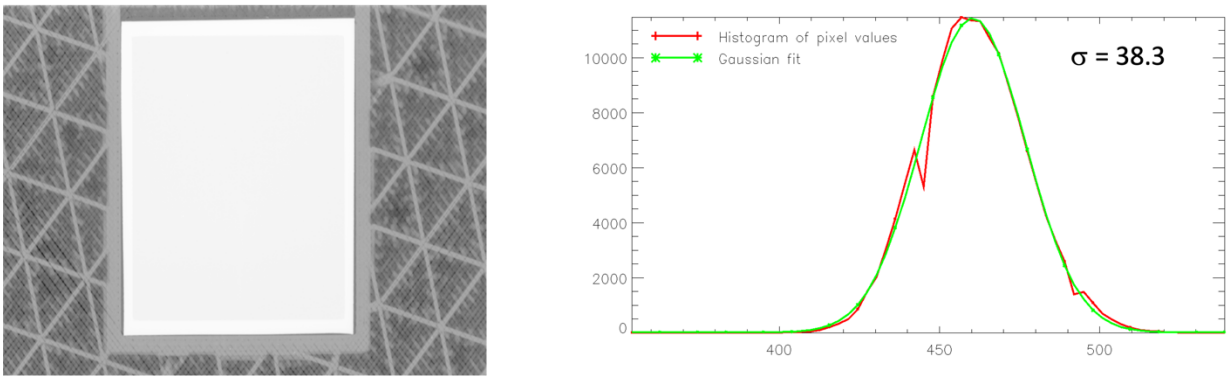


**Figure 7: Uniform data on image plates along with a histogram quantifying uniformity.**

Another measure of signal uniformity was to observe a lineout taken across the image. The lineout visually demonstrates how the signal level changes with respect to position. Figure 8 shows one sample dataset and lineout, where much of the signal is at approximately 470 gray scale units (GSU), with an increase of about 2% at the right edge. (GSU refers to the pixel value in a 16-bit gray scale image.) Most of the data collected for this work showed this level of uniformity; however, no threshold was determined to gauge acceptability. Instead, this plot was used as a "sanity check" to alert us if a measurement was grossly varying and needed to be retaken.

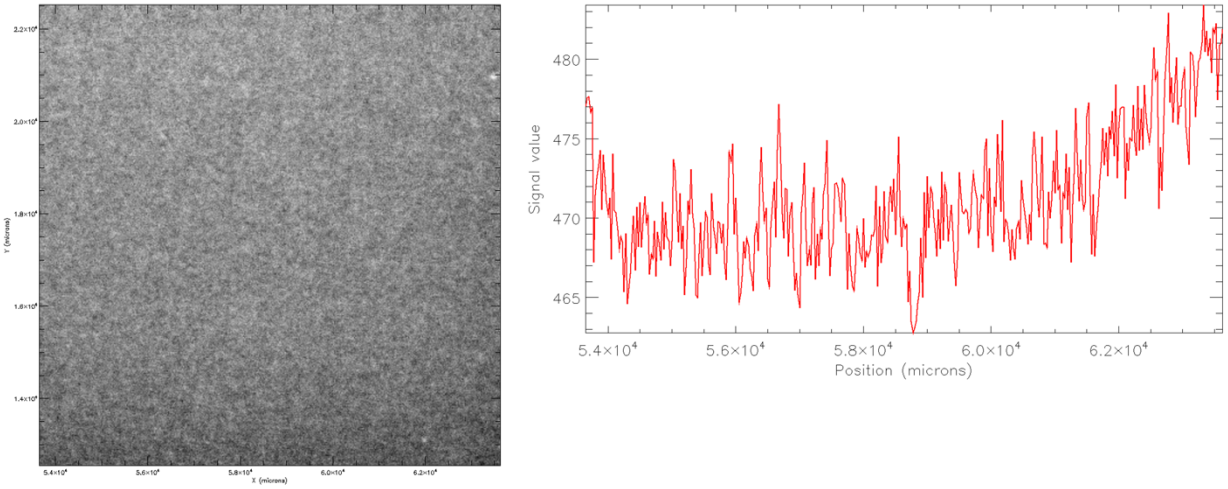


**Figure 8: Data region used for signal level calculation along with a lineout taken horizontally across the central 1000 microns to gauge acceptability of a measurement.**

# 3. DATA & RESULTS

Data from the cases described in Table 1 and Table 2 was collected over the course of several weeks. For each measurement the signal on the MCA was recorded on a computer, and the IP was scanned within 20 minutes of completing the exposure. Exposure times were long enough to record signal levels of at least 300 GSU above background to achieve acceptable signal-to-noise level in the IP data. In some cases, exposures longer than 1 hour were required to achieve the desired signal level due to thick filtering. Such long exposures sometimes caused the Manson source to break down and arc, rendering those measurements unusable due to the unknown effect of the breakdown on signal levels. Exposure times and applied voltages were adjusted as needed to balance run times and limit arcing. The lowest signals were around 460 GSU, though most were 1000 GSU or greater.

The measurements were processed to determine the weighted mean γ energy from the MCA spectrum and the mean GSU from the image plate data. In most cases 3 exposure sets were collected for each energy point, and the reported value is an average of these multiple measurements.

The quantity of GSU per count was computed for each dataset. This ratio measures the signal recorded by the image plate relative to the counts recorded by the MCA. We assume the conditions for each measurement were the same, providing a measure of scanner response as a function of γ energy. The conditions we assume were unchanged include the distance from source to both detectors, the area measured in the image plate, the pinhole size on the MCA, the gain setting of the MCA, and the alignment of the detectors to the source.

For each group of 3 measurements, the same 3 IP's were used. As a precaution, the IP's were numbered and tracked, as each IP does have a unique response. Typically, most IP's have similar responses; however, sensitivity between different pieces can vary by 10% or more. We noted no such trends for this work.

The efficiency of the MCA detector at the weighted mean x-ray energy was used to correct the count value by accounting for the detector efficiency at that energy, yielding the final metric of efficiency corrected response in GSU per count. 1-σ errors in the raw GSU values ranged from 4 to 9% which represents the spread in uniformity of the signal recorded on the image plates. The 1-σ errors for the response values shown in Table 3 represent the spread in the individual measurements.

**Table 3: Mean energy and efficiency corrected response for each group of data points**

| Anode | Filter | Mean γ energy (eV) | Avg. Eff. Corr. Response (GSU/count) |
|---|---|---|---|
| Al | 25 μm Al | 1487 | 1.55E-02 (±1%) |
| Ag | 10 μm Ag | 3162 | 2.41E-02 (±7%) |
| Ti | 60 μm Ti | 4555 | 3.28E-02 (±1%) |
| Fe | 100 μm Fe | 6639 | 3.98E-02 (±3%) |

| Anode | Filter | Mean γ energy (eV) | Avg. Eff. Corr. Response (GSU/count) |
|---|---|---|---|
| Cu | 100 µm Ni | 8012 | 5.28E-02 (±1%) |
| Zn | 75 µm Zn | 8756 | 4.37E-02 (±8%) |

A plot of the response as a function of incident γ energy shows the expected trend of increasing response with energy over the energy range of data collected. The data points (green circles) presented in Figure 9 are compared against the expected modelled response curve for Fuji TR IP. The intent is to match the shape of the response rather than to measure the absolute response directly from the data points collected. The absolute calibration of the MCA detector is unknown, and we take the count values from that detector to be relative. However, we assume that the response in counts, corrected for detector response, is consistent across this energy range; therefore, it is reasonable to assume the trend shown is correct.

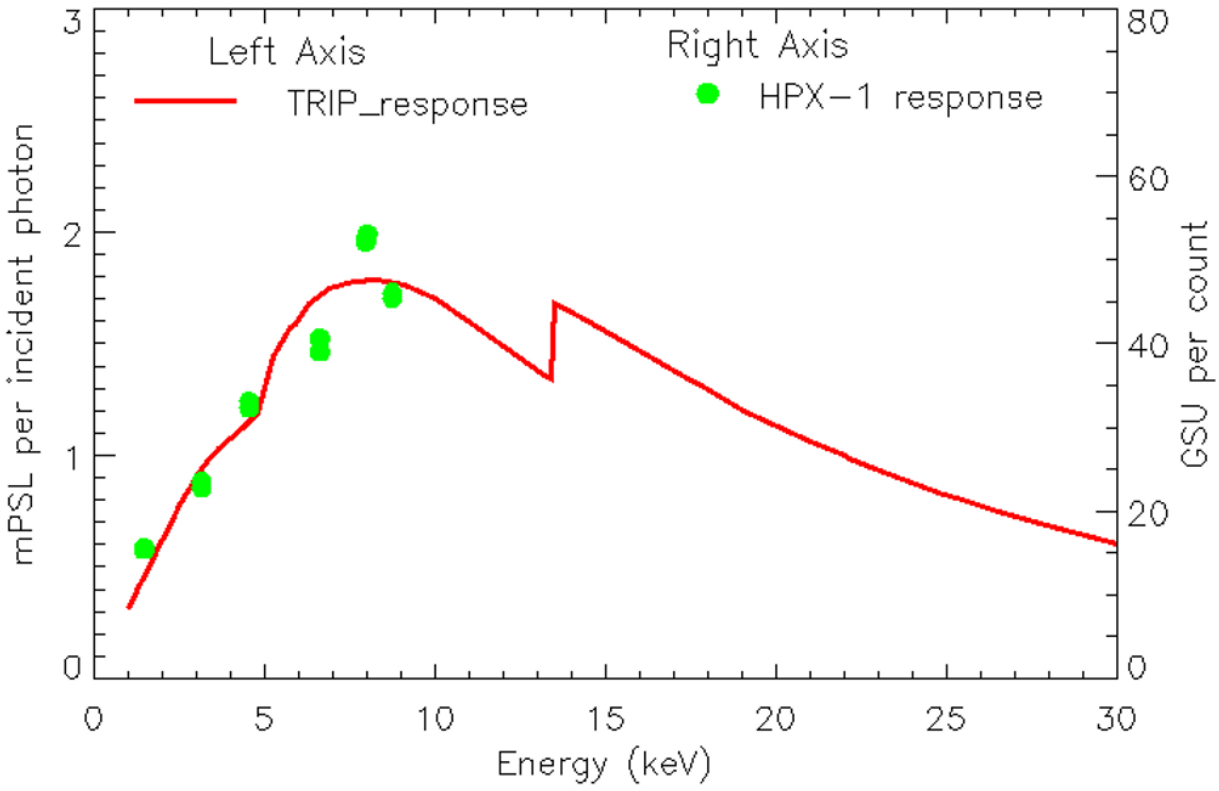


**Figure 9: Response measurements from a ratio of IP signal to MCA counts compared to the expected shape of the modelled response curve.**

The response curve included in Figure 9 is slightly different than previous examples. Specifically, the response published by Meadowcroft et al. [3] compared to the model used in this work shows slight

differences. Figure 11 presents a comparison of the two responses, normalized to their respective peak response values. The two primary differences are the peak response shifted slightly to higher energy from 5.9 keV to 8.1 keV, and the response remains higher in the MCNP6 model from the peak out to approximately 20 keV. The newer MCNP6 model was provided by N. Izumi through private communication. This model represents image plates as 6 layers, where the depth to which the scanning laser penetrates into the IP is a variable optimized to fit experimental data from radioisotope (RI) sources using the Izumi method [4]. Meadowcroft's response is a piece-wise fit to experimental data collected over four distinct energy ranges collected from different x-ray sources.

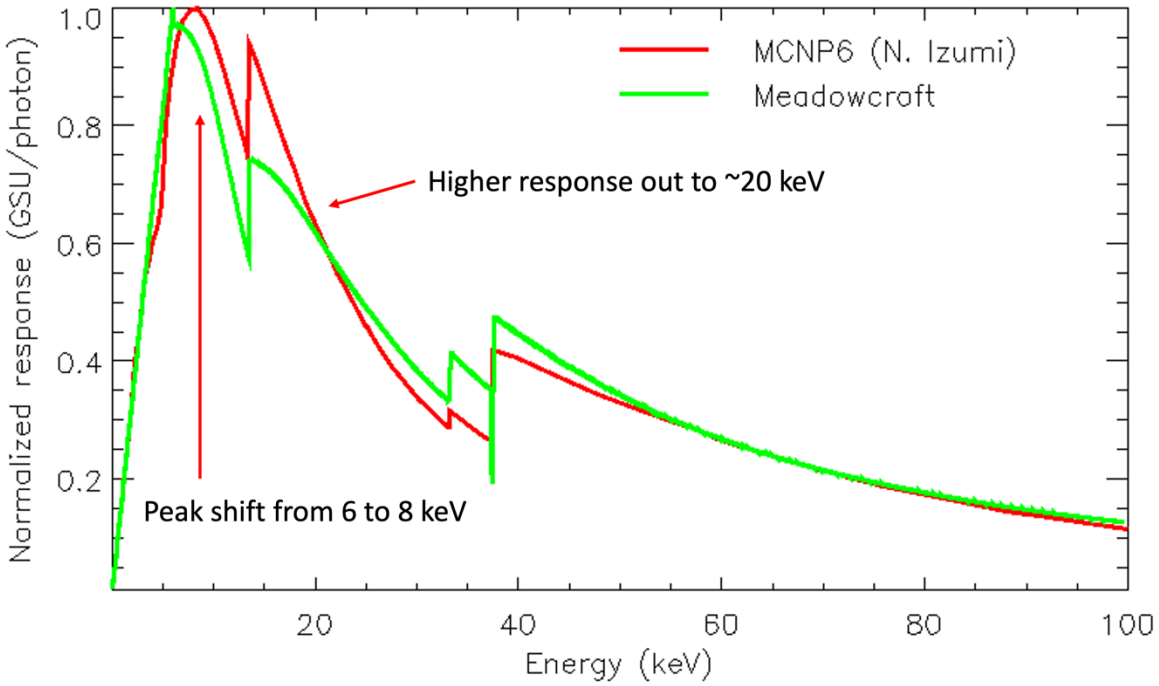


**Figure 10: Response of the HPX-1 scanner scaled to match GSU per incident photon values from RI sources.**

NIST-certified RI sources were used to determine the absolute scaling of the response curve. The RI sources are the M-type reference and calibration sources from Eckert &Ziegler. These consist of a salt deposited on a substrate, covered by a thin Mylar window, and contained in a 1-inch diameter disc, approximately the size of a quarter. The RI sources used in this work are Fe-55, Cd-109, and Am-241, with characteristic emissions at 5.9 keV, 22 keV, and 59 keV, respectively, in the order these sources are listed.

In 2013, a method utilizing these radioisotope (RI) sources was proposed by N. Izumi to calibrate the image plate (IP) scanning systems at NIF, LLE, and Z. [4] However, for the DITABIS scanner used at Z, results were inconsistent, and repeated attempts to calibrate the scanner led to further confusion. The hypothesis was that because the laser energy for the DITABIS scanner was approximately four times lower than that of the Fuji FLA7000 scanners used at NIF and LLE, the response of the scanning system was different. Due to the lower laser power, laser penetration into the IP to generate photo-stimulated emission was also reduced, leading to decreased photo-stimulated emission sensitivity, less scattering, and lower signal levels.

The calibration method proposed by Izumi required a 5-minute exposure at specific standoff distances of a few centimeters between each source and the image plate. However, with the DITABIS scanner, the signal levels measured according to this prescription were not sufficiently above background, necessitating much longer exposure times to generate a useful signal-to-noise ratio. The extended exposure times introduced additional uncertainty due to subsequent signal decay and fading during the multi-hour exposure process. Ultimately, the results never aligned with the expected response, and this approach was eventually abandoned.

Initial attempts to use this method for the Carestream HPX-1 system initially showed a sensitivity which was even lower than the DITABIS. Working with the manufacturer we increased the scanner sensitivity by an order of magnitude. Expecting problematic results from the Izumi method a direct contact exposure was attempted instead. This allowed for increased signal with short exposure times. The direct contact measurements showed reasonable results with acceptable signal-to-noise.

Figure 11 shows the MCNP6 model response scaled to match the GSU per incident γ determined using the Fe-55 RI source. Results from the Cd-109 and Am-241 sources indicate that the response could be higher or lower by less than a factor of 2. Scaling of the modelled response to match all three measurements simultaneously was not attempted. The RI sources come with a 2-year certification, which expired in 2019. The decay of the sources could be a reason for the deviation from the model. Another possibility is that the model was created for TR IP using the Fuji FLA7000 scanners at NIF, and the energy deposition profile of that scanner is likely different from the HPX-1. While the MCNP6 model could be optimized to fit this data, this was not pursued.

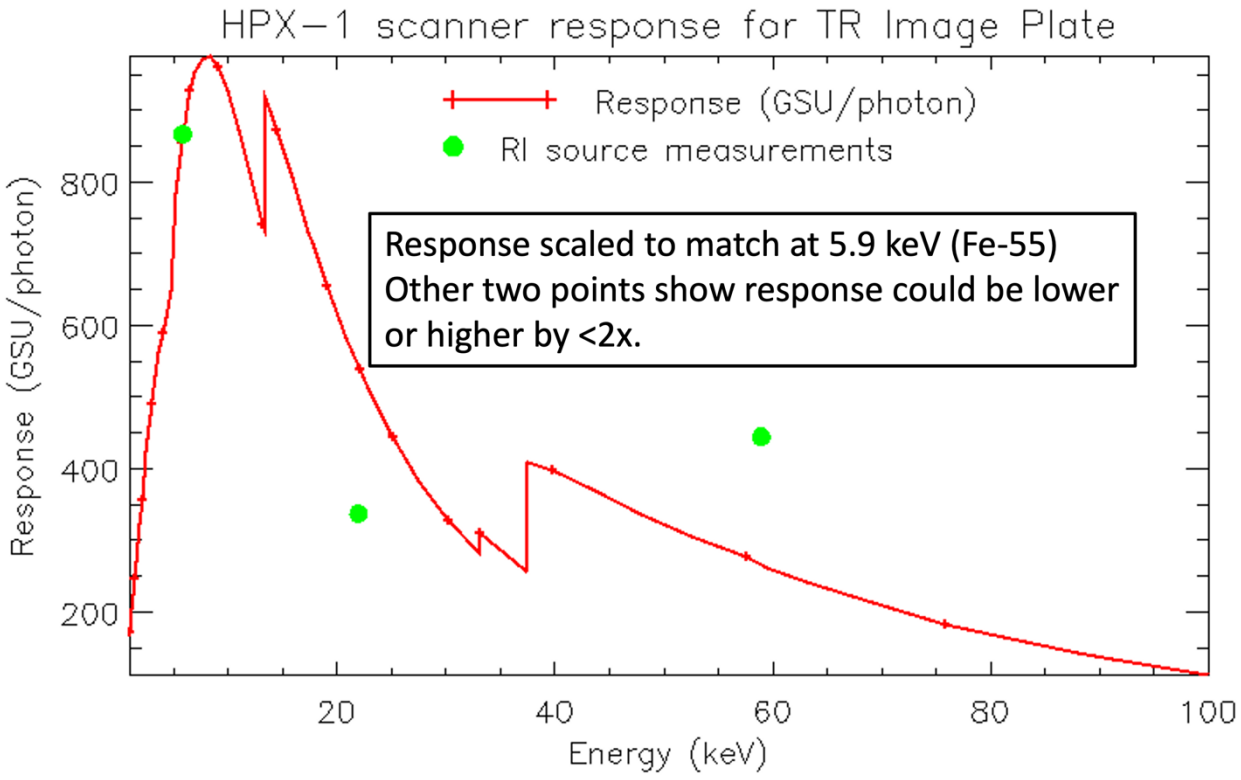


**Figure 11: Response of the HPX-1 scanner scaled to match GSU per incident photon values from RI sources.**

Because this calibration process applied to the HPX-1 scanner was successful, it was repeated for the unclassified DITABIS scanner. Results showed similar agreement, but there were issues.

One issue with the DITABIS calibration was that the measured response from the MCA-IP sensitivity determination followed the expected trend up to the Ti measurement at 4.6 keV, then deviated for the higher energy points. Figure 12 shows the data points in blue along with the expected responses from Meadowcroft and Izumi. Although the trend agrees up to Fe, the measured response appears to drop significantly for the Cu and Zn measurements. The agreement at Fe is questionable. We hypothesize that the IP scanner response changed, as the Cu and Zn points were taken approximately 1 week after the Al-Fe points (1.4-6 keV). Both model responses are shown to clarify that the drop in sensitivity for Cu and Zn is much greater than either model response predicts.

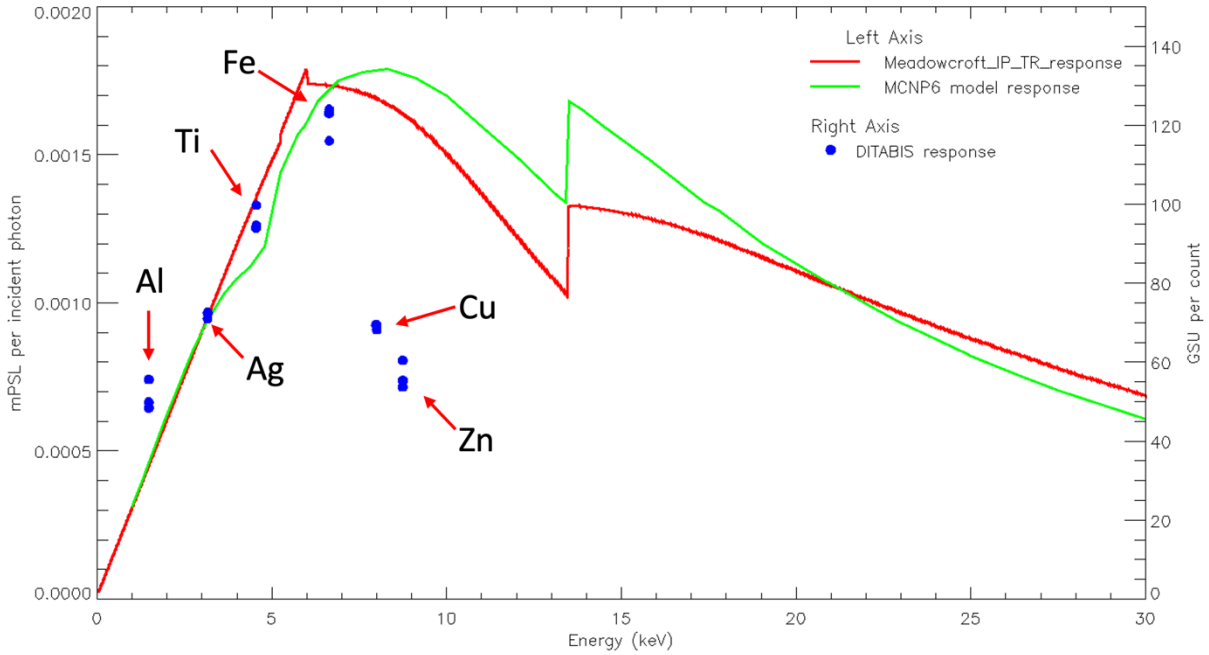


**Figure 12: Response of the DITABIS IP scanner compared to modelled responses.**

Scaling the Cu and Zn points by 2.31 forces these points to align with the expected trend, as shown in Figure 13 as magenta points. It is not clear why or how the DITABIS response can change over time, but this result suggests one possible explanation. Considering the DITABIS scanner's have been in service for over a decade, it is not surprising to expect electronics, such as the photo-multiplier tube, could exhibit degraded or fluctuating performance.

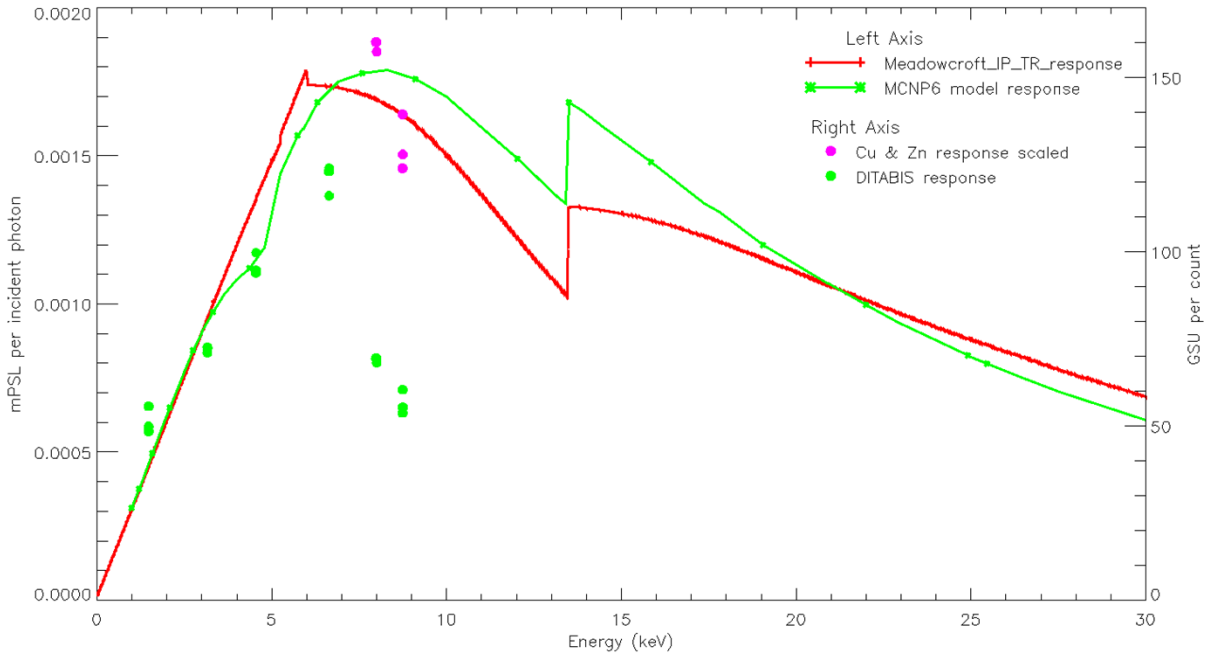


**Figure 13: Scaled response of the DITABIS IP scanner. As a demonstration the values for the Cu and Zn points were scaled up by 2.31 to match the expected trend.**

Further tests using the RI sources also indicated a change in the DITABIS scanner response. The results from two sets of measurements taken 4 days apart are shown in Figure 14. The red curve represents the MCNP6 model response scaled to match the initial measurement from the Fe-55 source at 5.9 keV. The green points are single measurements. The Cd-109 and Am-241 RI sources were measured and scanned 3 days after the Fe-55. The magenta points represent groups of 5 repeated measurements with 1-σ errors collected 1 day after the 2$^{nd}$ set of single measurements. The errors are 9%, 13%, and 4% for the measurements from the Fe-55 (5.9 keV), Cd-109 (22 keV), and Am-241 (59 keV) RI sources, respectively. Compared to the initial measurement, the response decreased by 9%, 58%, and 54% for the same ordering of energy points, respectively. These changes in scanner response, along with those noted for the MCA measurements, lead us to suspect the DITABIS scanner response varies significantly over time.

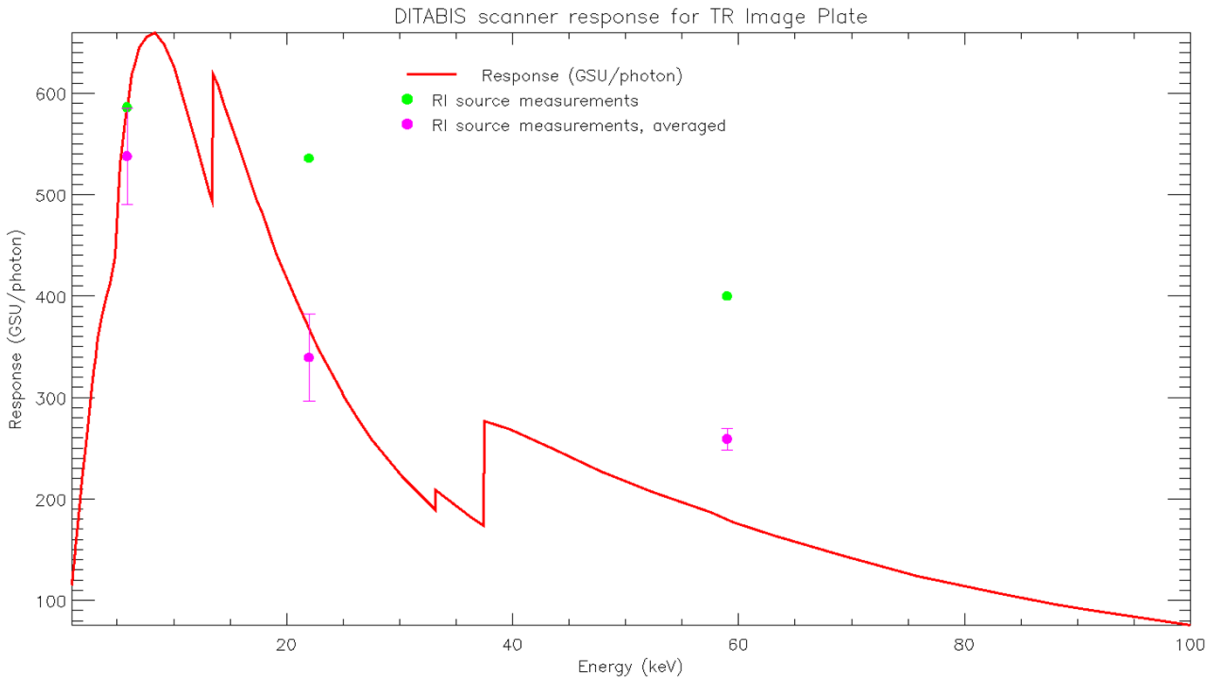


**Figure 14: Scaling measurements for the DITABIS IP scanner a step change. The green points are the initial measurement and represent a single value from each of the RI sources. The magenta points represent the average of 5 measurements from each RI source taken 4 days later.**

In contrast, repeat measurements using the HPX-1 scanner shows a remarkably stable response, as illustrated in Figure 15. The green points represent the initial individual RI source measurements taken 6 days apart, with the Fe-55 measurement taken first, followed by the Cd-109 and Am-241 measurements. The magenta points represent the same group of 5 repeated measurements taken 3 days after the Cd and Am single measurements. The error bars indicate the 1-σ error from averaging the 5 measurements. All measurements from the Carestream agree within the error bars, leading to the conclusion that the response of the Carestream HPX-1 scanning system is stable. We also conclude the HPX-1 is 50% more sensitive than the DITABIS based on the peaks of the scaled modelled response curves.

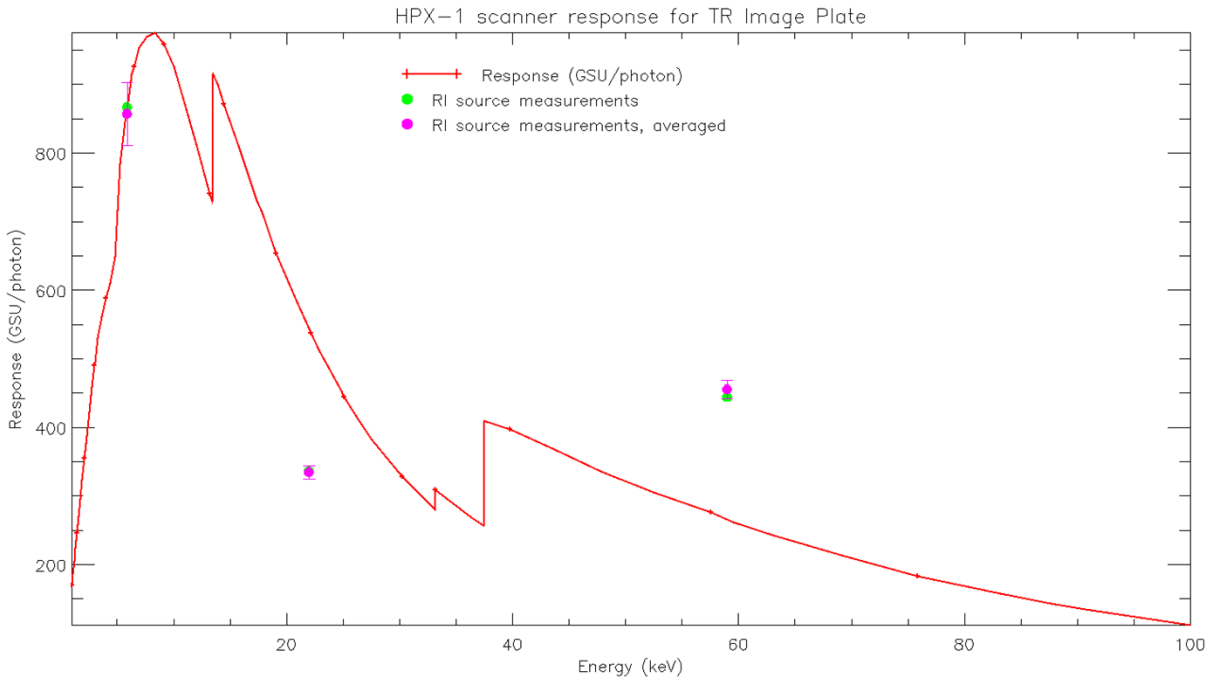


**Figure 15: HPX-1 scanner response for TR IP. Green points are single measurements. Magenta points represent the average of 5 repeated measurements along with the 1-σ error. All measurements lie within the error bars implying the HPX-1 system is stable and repeatable.**

# 4. SUMMARY AND FUTURE WORK

The response of both the Carestream HPX-1 and DITABIS image plate scanners were measured. Results show that the HPX-1 scanner is stable, while the DITABIS is not. From this work we provide an absolute measure of the HPX-1 response in GSU per incident photon as a function of energy. The response was measured in the range 1.47 keV– 8.75 keV and matched to a modeled response curve from MCNP6 extending out to 100 keV.

Further work could be undertaken to refine the MCNP6 model to more closely match the Carestream HPX-1 data. New RI sources could be procured to remove uncertainty from using sources which were out of calibration 6 years ago. Additional effort could also be directed toward understanding the MCA response for energies above 8.75 keV. Measurements with the MCA for energies above this value were inconclusive, though they would be valuable for further constraining the model fit, lending greater confidence to experimental spectra analyzed using this result.

# APPENDIX A. SUPPLEMENTAL CHARACTERIZATION WORK

## A.1. Carestream HPX-1 Characteristics

The HPX-1 scanner has the following characteristics:

- Laser power settings: high or low
- PMT settings: 10-100% in 10% increments
- Pixesl size: 25 μm, 50 μm, or 100 μm
- File format: DICONDE exported to 16-bit TIFF
- IP size: no restriction using a carrier plate
- Scan time: 66 seconds for all sizes used so far.

### Characterization Testing

A Manson source was used to expose image plates through a clear optical path 1951 Air Force Test Pattern. The test pattern was placed directly in front of the image plate using a test jig. For this work the Manson source used an aluminum anode with 10 kV voltage and 360 μA of current. Exposures were for 5 minutes. The test jig was placed on beam center inside of the vacuum test box at 24 inches from the source, as close as the jig could sit to the source. Two exposures were performed using two separate IP's. Scan were completed using the HPX-1 scanner within 1 hour of exposure. The 1st scan used the high laser power with PMT gain set to 100%. The 2nd scan was done at low laser power and PMT gain set to 50%. Analysis of the resulting image was performed to measure resolution from a sharp edge from the large block in the test pattern, the signal decay with repeated scans, and the contrast transfer function using the line-pair sets in the test pattern. Figure 16shows a sample exposure.
The scanner resolution was measured using the large square block on the left side of Figure 16. A lineout was taken across the sharp edge of both the horizontal and vertical faces. This lineout represents the Edge Spread Function (ESF). The derivative of the ESF yields the Line Spread Function (LSF) from which the FWHM is used as a quantifiable metric of scanner resolution. Figure 17 shows the lineouts used for the calculation.

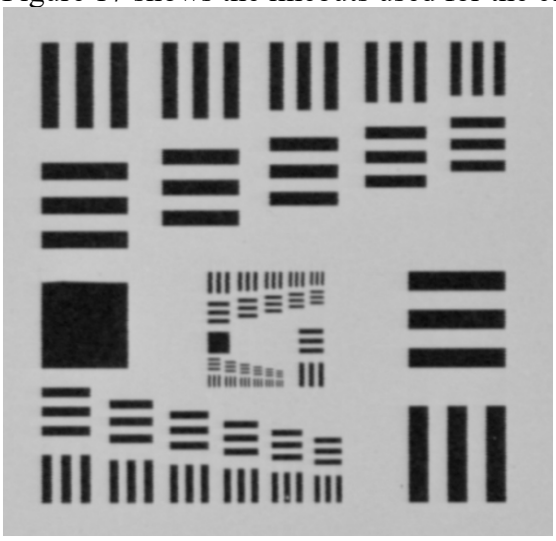

**Figure 16: 1951 AFTP used for characterization testing.**

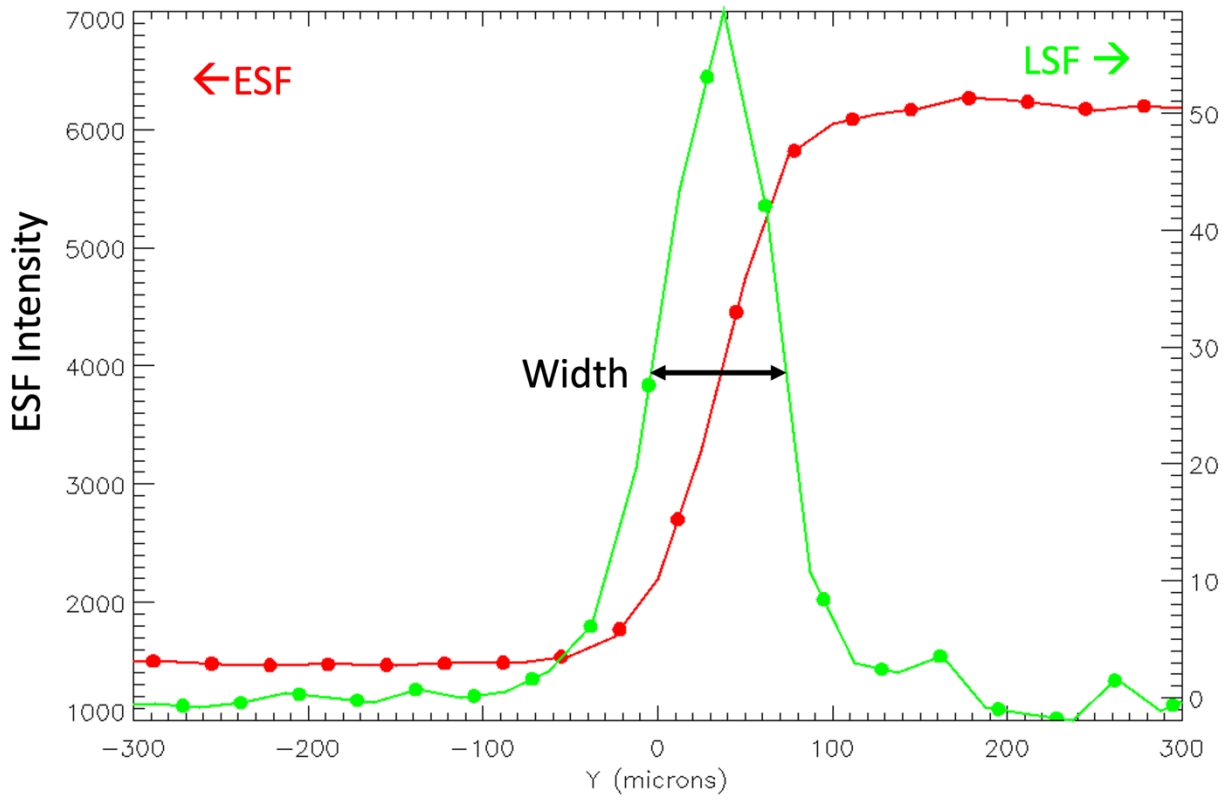


**Figure 17: ESF and LSF.**

Lineouts for both the low and high laser power scans were analyzed. Results are shown in Table 4. Note the low laser power condition is achieved by inserting a ND 1.5 filter into the laser path. No degradation in signal quality is expected.

**Table 4: Measured vertical and horizontal resolution values for the HPX-1 scanner.**

| Laser power | Horizontal resolution (μm) | Vertical resolution (μm) |
|---|---|---|
| High | 82.1± 3.8 | 78.2 ±2.7 |
| Low | 95.5 ±8.0 | 78.7 ±2.5 |

The image plates were scanned 5 times in a row to measure the reduction in signal level. The first signal was taken as the baseline and reported as 100%. The subsequent scans are reported as the 2$^{nd}$ – 5$^{th}$ scans. Figure 18 shows lineouts taken across the uniform square region. Signal levels were measured as the average signal across the higher flat region at positions greater than 0 on the x-axis. Note that all repeated scans were adjusted to match one another in position. Scan-to-scan registration in not repeatable for the HPX-1 scanner.

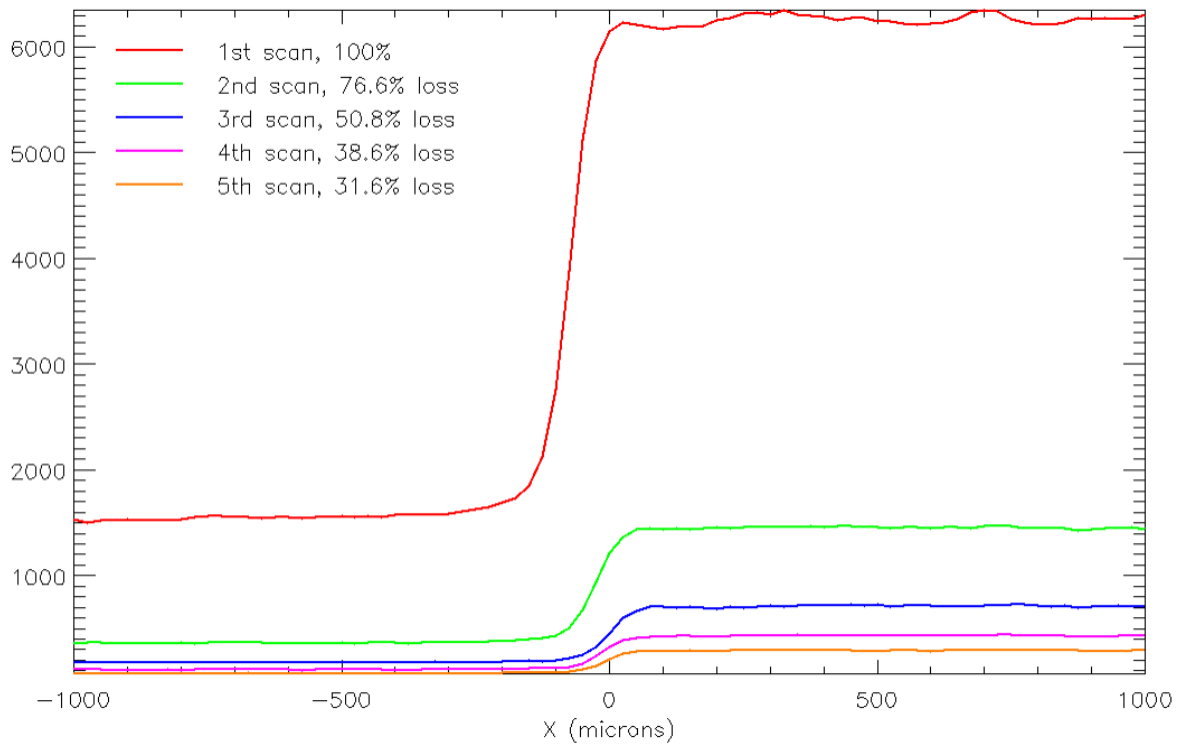


**Figure 18: Lineout data used to measure signal decay with repeated scans.**

Signal-to-noise was also measured using the uniform region within the square region on the left side of the test pattern. The quantity SNR was determined as the mean signal value over the standard deviation of those values, or SNR = $\mu/\sigma$. The change in SNR from repeated scans was also quantified, as shown in Table 4.

**Table 5: Signal-to-noise values for each laser setting as a function of repeated scan number.**

| Laser setting | Scan 1 | Scan 2 | Scan 3 | Scan 4 | Scan 5 |
|---|---|---|---|---|---|
| High | 49 | 45 | 36 | 31 | 26 |
| Low | 29 | 27 | 27 | 24 | 25 |

The SNR changes depending on where it is measured meaning the values present in should be taken as relative values for the sake of comparison. A comparison of CRITR data from scans on the Carestream HPX-1, the DITABIS, and the Typhoon FLA7000 scanners shows SNR values of 10.5%, 5.0%, and 14.6%, respectively. What is significant is the ration between the 3 systems, not the values themselves. The HPX-1 is about twice as noisy as the DITABIS but about half as noisy as the Typhoon FLA7000.

The contrast transfer function (CTF) was measured using the line pair sets in the test pattern. The CTF is defined as the ratio of the difference between the maximum and minimum signal values across a line-pair set over the sum of the same values.

$$CTF = \frac{Ymax - Ymin}{Ymax + Ymin}$$

Figure 19 shows a sample lineout region and corresponding data used in the calculation.

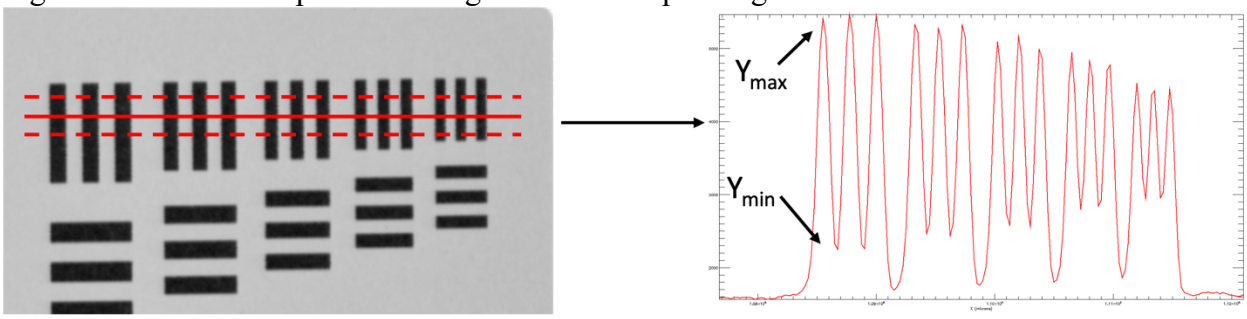


**Figure 19: Sample line-pair data and associated lineout.**

The CTF for each line pair set is plotting against each line-pair spacing value, as shown in Figure 20. The 10% threshold value is denoted by a black dashed line. Below this level details in the data cannot easily be distinguished. It is one approach to quantifying the useful limit of a scanners resolution. Compared to the DITABIS the HPX-1 scanner shows details below about 100 microns will be difficult to distin guish.

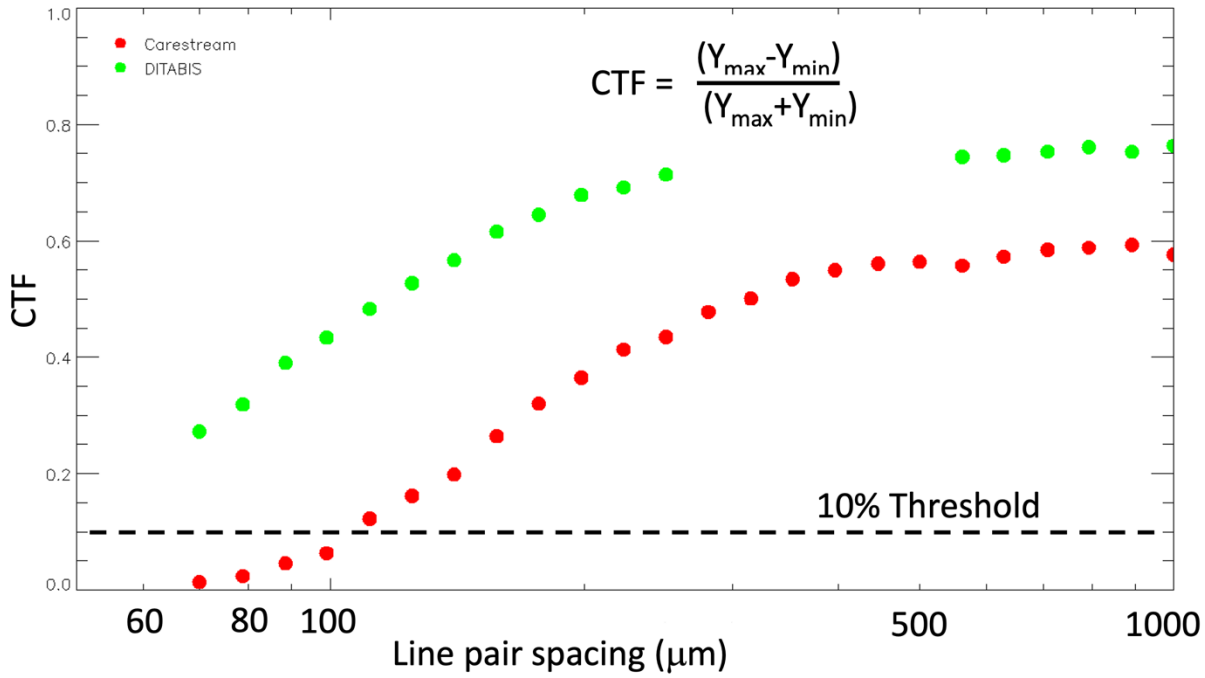


**Figure 20: CTF for the HPX-1 scanner compared with the DITABIS.**

The fade characteristics of the scanner for IP's left stored in a lab space over time were measured. Direct contact exposures of radio isotope sources were repeated many times then labelled with the respective exposure time and dates. A baseline set of measurements were exposed and scanned immediately. Over a period of a week multiple sets of data were scanned. Each later scan result was compared with the baseline value to determine a decay level. Up to four repeat measurements were made for each fade time. Figure 21 shows the result. The embedded table within Figure 21 provides a quick look at how much signal will decay over a

reasonable time period after a Z shot. For example, data scanned within 2 hours will have about 71% of its original signal level remaining while data left over a long weekend may only have about 42% remaining. A two-part exponential fit is used to calculate fade at a specific scan time after exposure.

$$F(t) = 0.274 * e^{-\frac{t}{27.7}} + 0.712 * e^{-t/8225.2}$$

The variable *t* is in minutes. A two-part fit was used because we expect there is an early time faster decay followed by a slower long component, where early time is expected to be < 30 minutes.

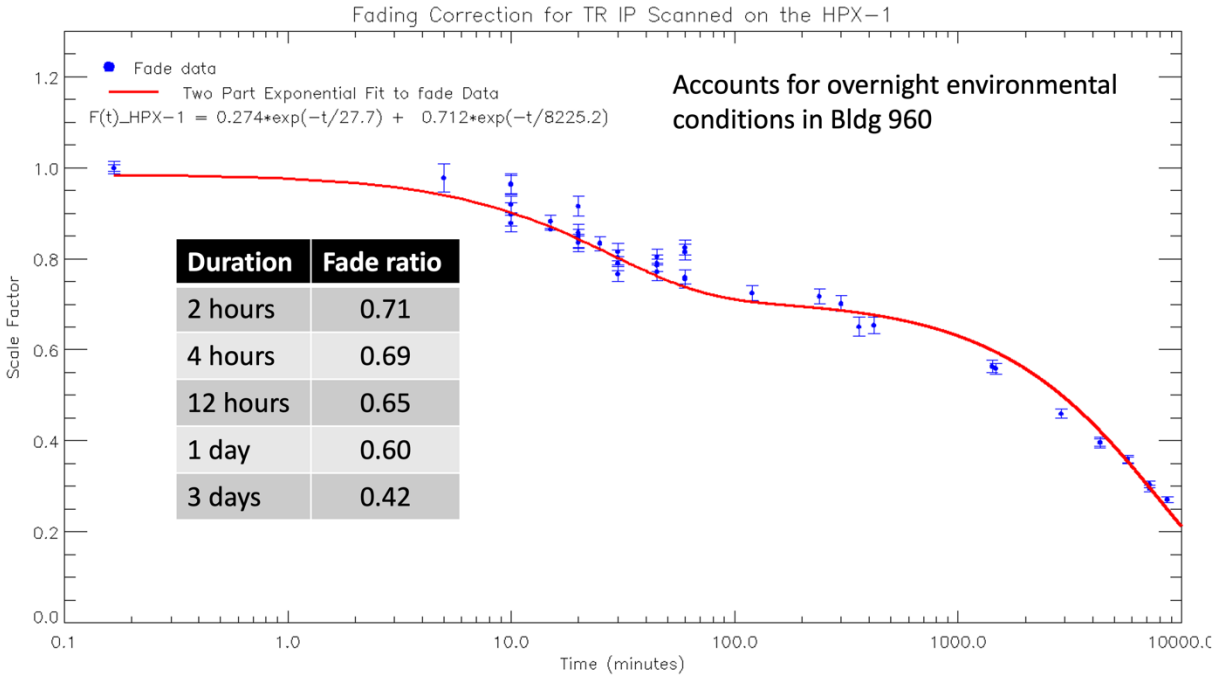


**Figure 21: Fade curve measured for the HPX-1.**

The fade data accounts for fade at normal room temperature in the scanning lab over the period of 1 week. This work could be re-peated for samples kept in the freezer to minimized signal decay over longer periods of a weekend.

## REFERENCES


[1] Haugh, M., J. Lee, E. Romano, M. Schneider, “Calibrating Image Plate Sensitivity in the 700. To 5000 eV Spectral Energy Range.” Proc. of SPIE Vol. 8850 885007-1, 2013.

[2] Rosenberg, M., D. B. Thorn, N. Izumi, D. Williams, M. Rowland, G. Torres, M. Haugh, P. Hillyard, N. Adelman, T. Schuler, M. A. Barrios, J. P. Holder, M. B. Schneider, K. B. Fournier, D. K. Bradley, S. P. Regan. “Image-plate sensitivity to x rays at 2 to 60 keV.” Rev. Sci. Instrum. 90, 013506, 2019.

[3] Meadowcroft, A. L., C. D. Bentley, E. N. Stott. “Evaluation of the sensitivity and fading characteristics of an image plate system for x-ray diagnostics” Rev. Sci. Instrum. 79, 113102, 2008

[4] N. Izumi, J. Lee, E. Romano, G. Stone, B. Maddox, T. Ma, V. Rekow, D. K. *Bradley, P. Bell, "X-ray and neutron sensitivity of imaging plates."*, Proc. of SPIE Vol. 8850 885006-1, 2013

Meadowcroft, A. L., Bentley, C. D., Stott, E. N., “Evaluation of the sensitivity and fading characteristics of an image plate system for

## DISTRIBUTION

**Email—Internal**

| Name | Org. | Sandia Email Address |
|---|---|---|
| Eric Harding | 1681 | ehardi@sandia.gov |
| Tim Webb | 1681 | tjwebb@sandia.gov |
| Brent Jones | 1688 | bmjones@sandia.gov |
| Antoinette Maestas | 1688 | aamaest@sandia.gov |
| Technical Library | 1911 | sanddocs@sandia.gov |

This page left blank

Sandia National Laboratories

Sandia National Laboratories is a multimission laboratory managed and operated by National Technology & Engineering Solutions of Sandia LLC, a wholly owned subsidiary of Honeywell International Inc. for the U.S. Department of Energy's National Nuclear Security Administration under contract DE-NA0003525.